A Lobatto interpolation grid over the triangle

2 authors, including:

M. G. Blyth
University of East Anglia
67 PUBLICATIONS   **1,262** CITATIONS

A Lobatto interpolation grid over the triangle

M. G. BLYTH†

School of Mathematics, University of East Anglia, Norwich NR4 7TJ, UK

AND

C. POZRIKIDIS‡

*Department of Mechanical and Aerospace Engineering,
University of California, San Diego, La Jolla, CA 92093-0411, USA*

A sequence of increasingly refined interpolation grids over the triangle is proposed, with the goal of achieving uniform convergence and ensuring high interpolation accuracy. The number of interpolation nodes, N, corresponds to a complete mth-order polynomial expansion with respect to the triangle barycentric coordinates, which arises by the horizontal truncation of the Pascal triangle. The proposed grid is generated by deploying Lobatto interpolation nodes along the three edges of the triangle, and then computing interior nodes by averaged intersections to achieve three-fold rotational symmetry. Numerical computations show that the Lebesgue constant and interpolation accuracy of the proposed grid compares favorably with those of the best-known grids consisting of the Fekete points. Integration weights corresponding to the set of Lobatto triangle base points are tabulated.

1. Introduction

We consider the polynomial interpolation of a function of two variables over a triangular domain with straight or curved edges in the xy plane. To standardize the problem, we map the physical triangle from the xy plane to a right isosceles triangle in the $\xi\eta$ parametric plane, so that $0 \leqslant \xi \leqslant 1$ and $0 \leqslant \eta \leqslant 1-\xi$, and an arbitrarily chosen vertex is mapped to the origin. The interpolated function is then approximated with a complete mth-degree polynomial in ξ and η,

$$f(\xi, \eta) \simeq P_m(\xi, \eta) = \sum_{k=0}^{m} \sum_{l=0}^{m-k} a_{kl}\xi^k\eta^l, \qquad (1.1)$$

involving N unknown coefficients, a_{kl}, where

$$N = \binom{m+2}{2} = \frac{1}{2}(m+1)(m+2). \qquad (1.2)$$

These are computed by selecting N interpolation nodes over the area of the triangle (ξ_i, η_i), and enforcing the usual interpolation conditions

$$f(\xi_i, \eta_i) = P_m(\xi_i, \eta_i), \qquad (1.3)$$

for $i = 1, 2, \ldots, N$.

---

† Email: m.blyth@uea.ac.uk
‡ Email: cpozrikidis@ucsd.edu

To expedite the interpolation process, we introduce the Lagrange-like cardinal node interpolation functions, $\psi_i(\xi, \eta)$, for $i = 1, 2, \ldots, N$, with the property

$$\psi_i(\xi_j, \eta_j) = \delta_{ij}, \tag{1.4}$$

where δ_{ij} is the Kronecker delta. The interpolating polynomial may then be recast into the form

$$f(\xi, \eta) = \sum_{i=1}^{N} \psi_i(\xi, \eta) f_i, \tag{1.5}$$

where $f_i = f(\xi_i, \eta_i)$ are the specified or presumed-known function values at each of the N nodes. In this light, the interpolation problem reduces to obtaining expressions for each of the N cardinal functions, ψ_i, using conditions (1.4). Once this has been accomplished, the function itself can be interpolated at any point over the triangle and beyond using (1.5).

By analogy with the well-developed theory of 1D interpolation, we assess the convergence of the 2D interpolation in terms of the Lebesgue constant, Λ_N, defined as

$$\Lambda_N = \max_{\mathbf{x} \in T} \{\mathcal{L}_N(\mathbf{x})\}, \tag{1.6}$$

where the point $\mathbf{x} = (\xi, \eta)$ lies on the standard triangle, T, and $\mathcal{L}_N$ is the Lebesgue function,

$$\mathcal{L}_N(\mathbf{x}) = \sum_{i=1}^{N} |\psi_i(\mathbf{x})|. \tag{1.7}$$

The convergence of the interpolation with respect to m or N depends on the functional dependence of the Lebesgue constant on N.

Now, to compute the cardinal node interpolation functions, we introduce a set of N polynomial functions, $\phi_j(\xi, \eta)$, that form a complete base of the mth-order polynomial space, as will be discussed below, and introduce the expansion

$$\psi_i(\xi, \eta) = \sum_{j=1}^{N} c_j^i \phi_j(\xi, \eta), \tag{1.8}$$

where c_j^i are unknown coefficients. Enforcing the conditions (1.4), we find that the vector of coefficients $\mathbf{c}_i = (c_1^i, \ldots, c_N^i)^\top$, corresponding to the ith cardinal function, satisfies the generalized Vandermonde system

$$\mathbf{V} \cdot \mathbf{c}_i = \mathbf{e}_i, \tag{1.9}$$

where $\mathbf{e}_i = (0, \ldots, 0, 1, 0, \ldots, 0)^\top$ and the unit resides in the ith position. The (k, j) entry of the generalized $N \times N$ Vandermonde matrix, $\mathbf{V}$, is given by $V_{kj} = \phi_j(\xi_k, \eta_k)$. Once the solution of the linear system (1.9) has been found, the polynomial interpolation over the triangle may be constructed according to (1.5).

In contrast to 1D interpolation, existence and uniqueness of the solution of (1.9) are not guaranteed and taken for granted in practical applications. Moreover, the difficulty of solving the linear system hinges on the well-conditioning of the generalized Vandermonde matrix, which is sensitive to the choice of the base functions, ϕ_j. In practice, it is advantageous to employ a set of polynomial basis functions that enjoy orthogonal or near-orthogonality properties. Two suitable candidates are provided by the Proriol and Appell polynomials discussed next.

1.1 *Proriol polynomials*

To introduce the Proriol polynomials, we map the standard triangle to the standard square $-1 \leqslant \xi' \leqslant 1$, $-1 \leqslant \eta' \leqslant 1$, using Duffy's transformation,

$$\xi = \frac{(1 + \xi')(1 - \eta')}{4}, \quad \eta = \frac{1 + \eta'}{2}, \tag{1.10}$$

and its inverse

$$\xi' = \frac{2\xi}{1 - \eta} - 1, \quad \eta' = 2\eta - 1, \tag{1.11}$$

as illustrated in Fig. 1. The Proriol polynomials are then given by

$$\mathcal{P}_{kl} = L_k(\xi')\left(\frac{1 - \eta'}{2}\right)^k J_l^{(2k+1,0)}(\eta') = L_k(\xi')(1 - \eta)^k J_l^{(2k+1,0)}(\eta'), \tag{1.12}$$

where L_k is a Legendre polynomial and $J_l^{(2k+1,0)}$ is a Jacobi polynomial (Proriol, 1957). Note that the factor $(1 - \eta)^k$ cancels the denominator of $L_k(\xi')$ arising from the fraction on the right-hand side of the transformation rule for ξ' shown in (1.11). Accordingly, the Proriol polynomial, $\mathcal{P}_{kl}$, involves monomials of the form $\xi^p \eta^{(k-p+q)}$ with combined order $k + q$, where $p = 1, 2, \ldots, k$ and $q = 1, 2, \ldots, l$.

The first few Proriol polynomials are given by

$$\begin{aligned}
\mathcal{P}_{00} &= 1, \\
\mathcal{P}_{10} &= 2\xi + \eta - 1, \\
\mathcal{P}_{01} &= 3\eta - 1, \\
\mathcal{P}_{20} &= 6\xi^2 + 6\xi\eta + \eta^2 - 6\xi - 2\eta + 1, \\
\mathcal{P}_{11} &= (2\xi + \eta - 1)(5\eta - 1), \\
\mathcal{P}_{02} &= 10\eta^2 - 8\eta + 1.
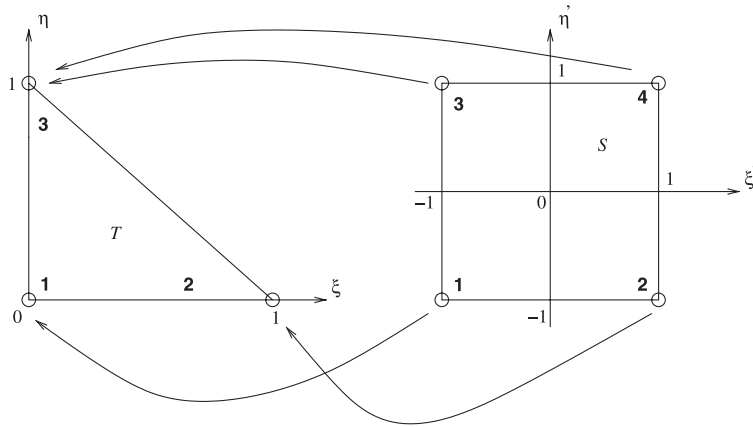\end{aligned} \tag{1.13}$$

FIG. 1. Mapping of the standard triangle to the standard square using Duffy's transformation.

Note that $\mathcal{P}_{00}$, $\mathcal{P}_{01}$, $\mathcal{P}_{02}$, ... are pure polynomials in η, whereas $\mathcal{P}_{10}$, $\mathcal{P}_{20}$, $\mathcal{P}_{30}$, ... are polynomials in both ξ and η. The properties of the Jacobi polynomials ensure that the Proriol polynomials satisfy the orthogonality relation

$$\iint_T \mathcal{P}_{ij}\mathcal{P}_{kl} \,\mathrm{d}\xi \,\mathrm{d}\eta = 0, \tag{1.14}$$

for $i \neq k$ and $j \neq l$. Thus, like the Fourier coefficients, the coefficients of a Proriol expansion can be computed readily by projection. The self-projection is given by

$$\mathcal{G}_{ij} \equiv \iint_T \mathcal{P}_{ij}\mathcal{P}_{ij} \,\mathrm{d}\xi \,\mathrm{d}\eta = \frac{1}{2(2i+1)(j+i+1)}. \tag{1.15}$$

Proriol polynomials provide us with a complete orthogonal basis. Any function, $f(\xi, \eta)$, defined over the standard triangle in the $\xi\eta$ plane can be approximated with a complete mth-degree polynomial in ξ and η, expressed in the form

$$f(\xi, \eta) \simeq \sum_{k=0}^{m}\left(\sum_{l=0}^{m-k} a_{kl}\mathcal{P}_{kl}(\xi, \eta)\right). \tag{1.16}$$

Multiplying (1.16) by $\mathcal{P}_{ij}$, integrating over the surface of the triangle, and using the orthogonality property, we find that the expansion coefficients are given by

$$a_{ij} = \frac{1}{\mathcal{G}_{ij}} \iint_T f(\xi, \eta)\mathcal{P}_{ij}(\xi, \eta) \,\mathrm{d}\xi \,\mathrm{d}\eta, \tag{1.17}$$

where $\mathcal{G}_{ij}$ is defined in (1.15).

To convert a monomial product series to the equivalent Proriol series, we use the expressions

$$\begin{aligned}
1 &= \mathcal{P}_{00}, \\
\xi &= \frac{1}{6}(3\mathcal{P}_{10} - \mathcal{P}_{01} + 2), \\
\eta &= \frac{1}{3}(\mathcal{P}_{01} + 1), \\
\xi^2 &= \frac{1}{30}(5\mathcal{P}_{20} - 3\mathcal{P}_{11} + 3\mathcal{P}_{02} - 4\mathcal{P}_{01} + 12\mathcal{P}_{10} + 5), \\
\xi\eta &= \frac{1}{60}(-3\mathcal{P}_{02} + 6\mathcal{P}_{11} + 6\mathcal{P}_{10} + 2\mathcal{P}_{01} + 5), \\
\eta^2 &= \frac{1}{30}(3\mathcal{P}_{02} + 8\mathcal{P}_{01} + 5).
\end{aligned} \tag{1.18}$$

1.2 Appell polynomials

The Appell polynomials are a generalization of the Jacobi polynomials to two dimensions, defined as

$$\mathcal{A}_{kl} = \frac{\partial^{k+l}}{\partial\xi^k \partial\eta^l}(\xi^k \eta^l \zeta^{k+l}), \tag{1.19}$$

where $\zeta = 1 - \xi - \eta$ is the third barycentric coordinate (e.g. Suetin, 1999). Carrying out the differentiations, we find that $\mathcal{A}_{kl}$ is a complete $(k + l)$-degree polynomial in ξ and η, given by

$$\mathcal{A}_{kl}(\xi, \eta) = k!l! \sum_{i=0}^{k} \sum_{j=0}^{l} (-1)^{i+j} \frac{(k)_i (l)_j (k + l)_{i+j}}{i!^2 j!^2} \xi^i \eta^j \zeta^{k+l-i-j}, \tag{1.20}$$

where $(p)_0 \equiv 1$, subject to the definition

$$(p)_q \equiv (-p)(-p + 1)(-p + 2) \cdots (-p + q - 1), \text{ for } q \geqslant 1,$$

for integers p and q; e.g. $(-1)_q = q!$. Alternatively, since $\mathcal{A}_{kl}$ is a $(k + l)$-degree polynomial, it can be presented in the form

$$\mathcal{A}_{kl}(\xi, \eta) = \sum_{i=0}^{k+l} \sum_{j=0}^{k+l-i} a_{kl,ij} \xi^i \eta^j, \tag{1.21}$$

with coefficients

$$a_{kl,ij} = (-1)^{i+j} \frac{(k + j)!(l + i)!}{i!^2 j!^2} \frac{(k + l)!}{(k + l - i - j)!}. \tag{1.22}$$

Note that, as required by symmetry, $a_{kl,ij} = a_{lk,ji}$. Using these formulae, we derive the first few Appell polynomials

$$\begin{aligned}
\mathcal{A}_{00} &= 1, \\
\mathcal{A}_{10} &= \zeta - \xi = 1 - 2\xi - \eta, \\
\mathcal{A}_{01} &= \zeta - \eta = 1 - 2\eta - \xi, \\
\mathcal{A}_{20} &= 2\zeta(\zeta - 4\xi) + 2\xi^2, \\
\mathcal{A}_{11} &= \zeta(\zeta - 2\xi - 2\eta) + 2\xi\eta, \\
\mathcal{A}_{02} &= 2\zeta(\zeta - 4\eta) + 2\eta^2.
\end{aligned} \tag{1.23}$$

It can be shown that the Appell polynomials satisfy the orthogonality condition

$$\iint_T \mathcal{A}_{kl}(\xi, \eta) \xi^p \eta^q \, d\xi \, d\eta = 0, \quad \text{for } p + q < k + l \equiv m. \tag{1.24}$$

Consequently, $\mathcal{A}_{kl}(\xi, \eta)$ is orthogonal to any polynomial of lower total degree in ξ and η, i.e. any polynomial involving monomials $\xi^p \eta^q$ with $p + q < k + l$.

2. High-order and spectral node distributions over the triangle

Much attention has been focused in the literature on the important question of optimal node distribution, with the goal of minimizing the interpolation error in accordance with some appropriate norm. In finite element solutions of second-order differential equations (e.g. Karniadakis & Sherwin, 2004), at least some nodes must be distributed at the triangle vertices and along the edges, so that C^0 continuity of the solution can be easily enforced across the element boundaries.
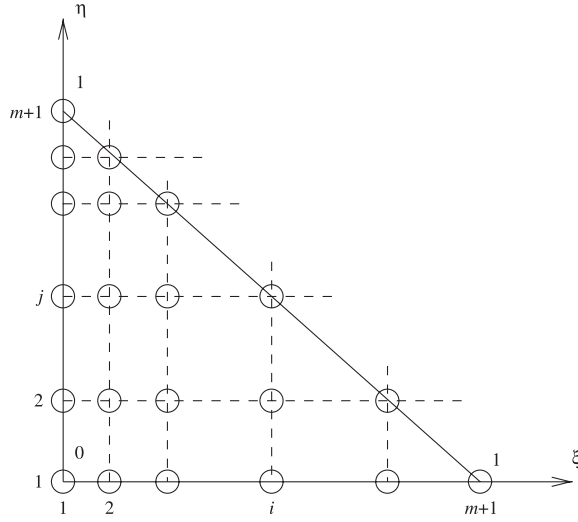
FIG. 2. Distribution of interpolation nodes corresponding to a complete mth-order polynomial expansion over the standard triangle, generated by an arbitrary 1D master grid.

To ensure that the number of interpolation nodes is equal to the number of coefficients in the complete mth-order expansion, we may deploy the nodes as shown in Fig. 2. Points on the ξ and η axes are placed at the nodes of a 1D *master grid* defined by a set of $m + 1$ points, v_i, where $i = 1, 2, \ldots, m + 1$, subject to the conditions $v_1 = 0$ and $v_{m+1} = 1$, so that the vertical and horizontal grid lines are described by

$$\xi_i = v_i, \quad \eta_j = 1 - v_{m+2-j}, \tag{2.1}$$

for $i, j = 1, \ldots, m + 1$. The nodes along the hypotenuse of the triangle are located by moving either vertically upward from the nodes on the ξ axis, or horizontally to the right from the nodes on the η axis. The interior nodes are placed at the intersections of the vertical and horizontal lines, yielding pairs (ξ_i, η_j), where $i = 1, \ldots, m + 1$ and $j = 1, \ldots, m + 2 - i$. Three possible choices for the master grid are discussed next.

2.1   Uniform grid

To obtain an evenly spaced grid, as illustrated in Fig. 3(a), we set $v_i = (i - 1)/m$, for $i = 1, \ldots, m + 1$. The diagonal lines correspond to constant values of the barycentric coordinate $\zeta = 1 - \xi - \eta$, ranging from $\zeta = 0$ to $\zeta = 1$ over the area of the triangle. Each diagonal line is identified by the index

$$k = m + 3 - i - j, \tag{2.2}$$

which decreases from the value of 1 along the hypotenuse to the value of $m + 1$ at the origin. Bos (1983) observed that the nodes fall around the perimeters of $[\frac{1}{3}(m - 1)] + 1$ nested triangles, where the square brackets denote the integral part. An example for $m = 10$ is shown in Fig. 3(b).

To construct the cardinal node interpolation functions, we observe that for each node, all other nodes lie on preceding horizontal and vertical lines and on following diagonal lines. We may then express the

(a)

(b)

FIG. 3. (a) Illustration of an evenly spaced grid over the triangle. (b) The interpolation nodes fall on a nested sequence of concentric triangles.

interpolation function for the (i, j) node as the product of three functions,

$$\psi_{ij}(\xi, \eta) = \Xi_i^{(i-1)}(\xi) \times H_j^{(j-1)}(\eta) \times Z_k^{(k-1)}(\zeta), \tag{2.3}$$

where:

- $\Xi_i^{(i-1)}(\xi)$ is an $(i-1)$-degree polynomial, defined such that

$$\Xi_1^0(\xi) = 1,$$
$$\Xi_i^{(i-1)}(\xi) = \frac{(\xi - v_1)(\xi - v_2)\cdots(\xi - v_{i-2})(\xi - v_{i-1})}{(v_i - v_1)(v_i - v_2)\cdots(v_i - v_{i-2})(v_i - v_{i-1})}, \tag{2.4}$$

for $i = 2, 3, \ldots, m+1$.

- $H_j^{(j-1)}(\eta)$ is a $(j-1)$-degree polynomial, defined such that

$$H_1^0(\eta) = 1,$$
$$H_j^{(j-1)}(\eta) = \frac{(\eta - v_1)(\eta - v_2)\cdots(\eta - v_{j-2})(\eta - v_{j-1})}{(v_j - v_1)(v_j - v_2)\cdots(v_j - v_{j-2})(v_j - v_{j-2})}, \tag{2.5}$$

for $j = 2, 3, \ldots, m+1$.

- $Z_k^{(j-1)}(\zeta)$ is a $(k-1)$-degree polynomial, defined such that

$$Z_1^0(\zeta) = 1,$$
$$Z_k^{(k-1)}(\zeta) = \frac{(\zeta - v_1)(\zeta - v_2)\cdots(\zeta - v_{k-2})(\zeta - v_{k-1})}{(v_k - v_1)(v_k - v_2)\cdots(v_k - v_{k-2})(v_k - v_{k-1})}, \tag{2.6}$$

for $k = 2, 3, \ldots$.

It can be confirmed that $\psi_{ij}(\xi, \eta)$ is a polynomial of degree $(i-1) + (j-1) + (k-1) = m$ with respect to ξ and η, as required, and that all cardinal interpolation conditions are met.

Unfortunately, as the expansion order m is increased, the accuracy over the uniform grid deteriorates due to the Runge effect. In particular, the interpolated function experiences large oscillations between nodes and the Lebesgue constant increases rapidly with N (Bos, 1983). Thus, the uniform node distribution is only suitable for low-order polynomial expansions, typically $m \leqslant 3$. To improve the interpolation accuracy, Bos (1983) cleverly modified the uniform node layout by expanding or contracting the individual sizes of the nested triangles while maintaining the uniformity of the point distribution around their perimeters.

2.2   Lobatto grid

A node distribution corresponding to the zeros of Lobatto polynomials is optimal for 1D interpolation, subject to the constraint that one node is placed at the left-end and another node is placed at the right-end of the interpolation domain (Fejér, 1932; Pozrikidis, 2005). The ith Lobatto polynomial is defined as $\mathrm{Lo}_i(t) \equiv L'_{i+1}(t)$, where $L_{i+1}(t)$ is a Legendre polynomial and the prime denotes a derivative. Motivated by this rigorous result, we propose a heuristic master grid with interior nodes given by

$$v_i = \frac{1}{2}(1 + t_{i-1}), \tag{2.7}$$

for $i = 2, \ldots, m$, complemented by $v_1 = 0$ and $v_{m+1} = 1$. The points t_i are the zeros of the $(m-1)$-degree Lobatto polynomial, which are distributed over the interval $(-1, 1)$. An example for $m = 6$ is shown in Fig. 4(a). The boundary and interior nodes are identified by the coordinates $(\xi_i, \eta_j) = (v_i, v_j)$, where $i = 1, \ldots, m+1$, and $j = 1, \ldots, m+2-i$.

Figure 4(b) shows the same node distribution mapped onto an equilateral triangle with sides of unit length in the $\hat{\xi}\hat{\eta}$ plane. The mapping is mediated by the functions

$$\hat{\xi} = \xi + \frac{1}{2}\eta, \quad \hat{\eta} = \frac{\sqrt{3}}{2}\eta, \tag{2.8}$$
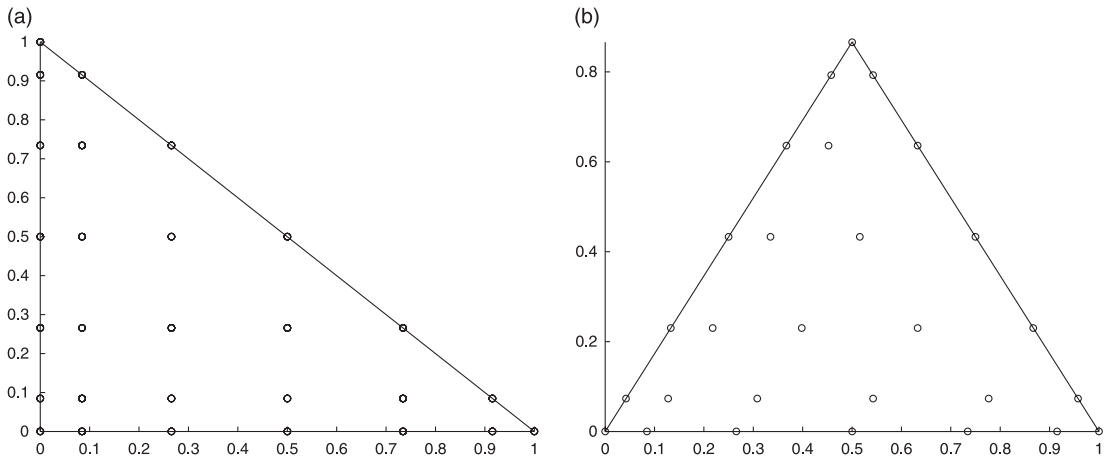

FIG. 4. (a) Lobatto grid for $m = 6$. (b) The same grid mapped onto an equilateral triangle.

and the inverse functions

$$\xi = \hat{\bar{\xi}} - \frac{1}{\sqrt{3}}\hat{\eta}, \quad \eta = \frac{2}{\sqrt{3}}\hat{\eta}. \tag{2.9}$$

The asymmetry of the distribution with respect to the three vertices is an unacceptable deficiency. An improved, symmetric node distribution is the main proposal of the present work, as will be discussed in Section 3.

2.3 *Fekete node distribution*

Another way of arranging the interpolation nodes over the triangle is provided by the Fekete points (Bos, 1983). To define these points, we apply the polynomial expansion (1.1) at $N = \frac{1}{2}(m+1)(m+2)$ nodes over the surface of the triangle (ξ_i, η_i), and consider the $N \times N$ generalized Vandermonde matrix featured in (1.9), regarded as a function of the nodal positions,

$$\mathbf{V}(\xi_1, \eta_1, \xi_2, \eta_2, \ldots, \xi_N, \eta_N). \tag{2.10}$$

By definition, the Fekete points maximize the magnitude of the determinant of the generalized Vandermonde matrix within the confines of the triangle. The significance of the Fekete points lies in the observation that the cardinal interpolation functions may be expressed in the form

$$\psi_i(\xi, \eta) = \frac{\det[\mathbf{V}(\xi_1, \eta_1, \xi_2, \eta_2, \ldots, \xi_{i-1}, \eta_{i-1}, \xi, \eta, \xi_{i+1}, \eta_{i+1}, \ldots \xi_N, \eta_N)]}{\det[\mathbf{V}(\xi_1, \eta_1, \xi_2, \eta_2, \ldots, \xi_N, \eta_N)]}, \tag{2.11}$$

for $i = 1, \ldots, N$. Expanding the determinant along the column involving ξ and η, we see that the numerator is an mth-degree polynomial in (ξ, η). When $\xi = \xi_j$ and $\eta = \eta_j$, with $j \neq i$, two rows of the generalized Vandermonde matrix become identical, and the numerator vanishes identically. Finally, we note that the right-hand side of (2.11) is equal to unity when $\xi = \xi_i$ and $\eta = \eta_i$ and conclude that (2.11) satisfies all the requirements of a cardinal function. In practice, the cardinal functions are computed by solving the Vandermonde system (1.9), identifying the base functions, ϕ_j, with the Proriol or Appell orthogonal polynomials previously discussed.

The Fekete node distribution is shown in Fig. 5 for $m = 6$, after Taylor *et al.* (2000). Remarkably, the vertex and edge nodes turn out to be located precisely at the zeros of the Lobatto polynomial, as conjectured earlier by Bos (1991). Moreover, the associated Lebesgue constant is found to be small. Typical values are given in Table 2.

By construction, the cardinal interpolation functions corresponding to the Fekete points satisfy

$$|\psi_i(\xi, \eta)| \leqslant 1, \tag{2.12}$$

with the equality holding when $\xi = \xi_i$ and $\eta = \eta_i$. This means that the Lebesgue constant defined in (1.6) is bounded from above by N. In fact, numerical evidence suggests that the upper bound is proportional to $\sqrt{N}$ (Taylor *et al.,* 2000). At present, the Lebesgue constant for the Fekete points is the lowest known constant for $m > 10$ (Taylor *et al.,* 2000).

Some intriguing observations can be made regarding the location of some of the Fekete points in a given set. Following the three broken lines emanating from the lower left-hand corner node in Fig. 5, we note that the pair of nodes intersected by the outer two broken lines are related to the Lobatto zeros
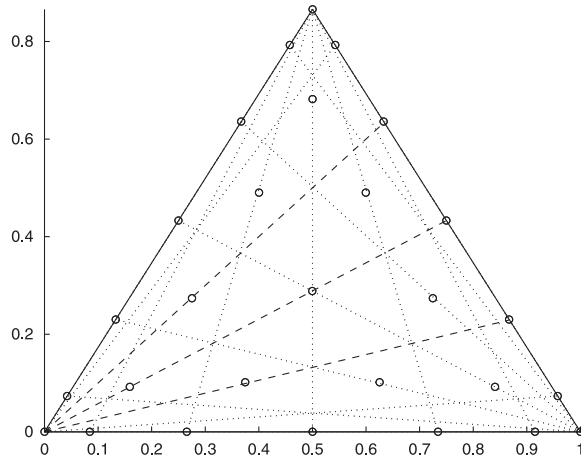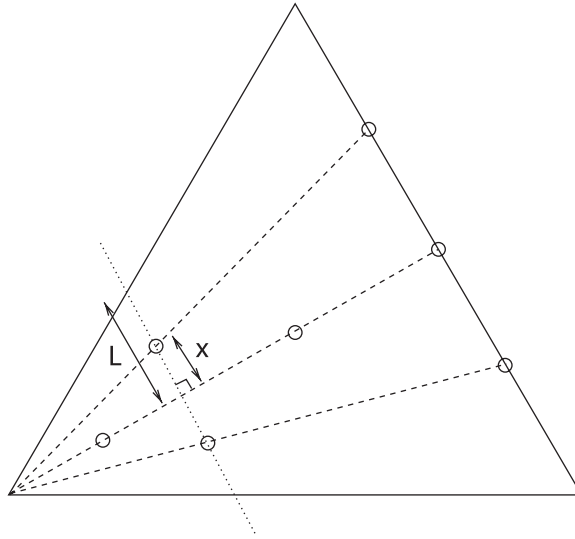
FIG. 5. The Fekete nodes for the case $m = 6$.

FIG. 6. Sketch showing the apparent connection between some of the Fekete nodes in Fig. 5 for $m = 6$, and the zeros of the Lobatto polynomial. When a dotted line is drawn through two of the nodes, we find that $x/L = 0.459$, which is approximately the same as the first zero of $\mathrm{Lo}_2(t)$, $t = 0.447$.

in the following sense. If an imaginary line is drawn through the nodes from the nearest two edges of the triangle perpendicular to the middle broken line, as illustrated in Fig. 6, the two Fekete nodes sit on this line, close to the two zeros of the second Lobatto polynomial, Lo_2, scaled by the length of the imaginary line. The near-corner node on the middle broken line lies midway between the edges of the triangle, and in this sense may be associated with the single zero of the first Lobatto polynomial, Lo_1, although this observation alone is not sufficient to determine the node position.

2.4 *Alternative schemes*

Other attempts have been made to compute optimal node distributions over the triangle. An alternative node pattern was developed by Chen & Babuška (1995), by minimizing the L_2 norm

$$\left\{ \iint_T \sum_{i=1}^{N} [\psi_i(\xi, \eta)]^2 \, d\xi \, d\eta \right\}^{1/2} \tag{2.13}$$

with respect to the nodal coordinates. Unlike the Fekete set, this distribution does not include edge nodes corresponding to zeros of the Lobatto polynomials. Hesthaven (1998) obtained small Lebesgue constants by minimizing an electrostatic energy function. Like the Fekete set, these distributions include edge nodes corresponding to the zeros of the Lobatto polynomials.

3. Lobatto grid over the triangle

For the Fekete points, the Chen and Babuška points and the Hesthaven points discussed in the previous section, the computation of the point distributions for a specified polynomial order, m, requires a fair amount of effort. It is desirable to devise a more practical method without overly compromising the interpolation accuracy. As a competitive alternative, we propose a Lobatto triangle distribution that is similar to that discussed in Section 2, but is endowed with three-fold rotational symmetry. In the proposed distribution, the nodal coordinates are given by

$$\xi_i = \frac{1}{3}(1 + 2v_j - v_i - v_k), \quad \eta_j = \frac{1}{3}(1 + 2v_j - v_i - v_k), \tag{3.1}$$

for $i = 1, 2, \ldots, m+1$, and $j = 1, 2, \ldots, m+2-i$, where $k = m+3-i-j$.

The distribution for $m = 6$ is illustrated in Fig. 7(a). It will be noted that the edge nodes remain in their original positions at the zeros of the Lobatto polynomial. Drawing a mesh of dotted lines connecting the edge nodes on the equilateral triangle, as shown in Fig. 7(b), we see that the interior nodes
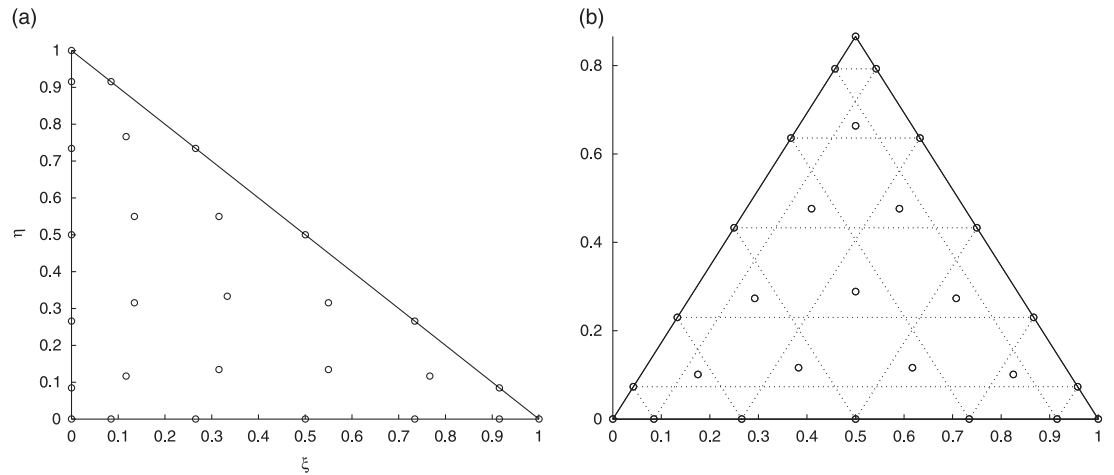

FIG. 7. Node arrangement with three-fold symmetry for $m = 6$ on (a) the standard Lobatto triangle in parametric $\xi\eta$ space and (b) the standard triangle mapped onto an equilateral triangle with sides of unit length.
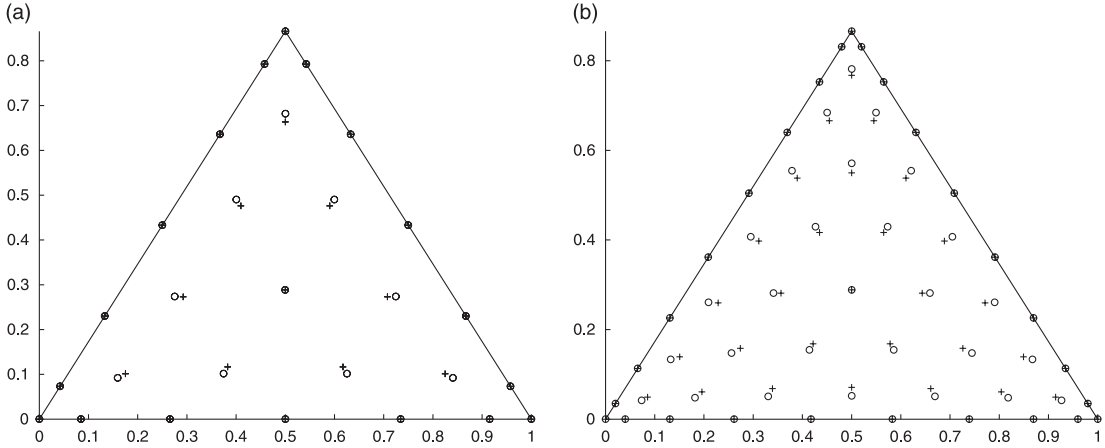
FIG. 8. Comparison of the Fekete nodes, shown as circles, with the Lobatto triangle nodes, shown as crosses, for (a) $m = 6$ and (b) $m = 9$.

are situated at the centroids of the smaller, inner triangles immediately surrounding them. In contrast, the interior nodes for the Lobatto grid discussed in Section 2.2 occur at the leftmost vertex of each of these inner triangles.

Before discussing the properties of the proposed symmetric Lobatto triangle distribution, we note the striking resemblance between the Fekete nodes and the Lobatto triangle nodes, as illustrated in Fig. 8 for the two cases $m = 6$ and $m = 9$. Nevertheless, we have confirmed that the determinant of the Vandermonde matrix for the Fekete nodes is somewhat larger than that for the Lobatto nodes.

3.1 *Properties of the Lobatto grid over the triangle*

Given the nodal distribution, the Lebesgue constant was computed using the method discussed in Section 2, where the Appell or Proriol polynomials were used as a basis for the cardinal interpolation functions. Specifically, the cardinal function expansion (1.8) is expressed in the form

$$\psi_i = \sum_{k=0}^{m} \sum_{l=0}^{m-k} b_{kl}^{(i)} \chi_{kl}(\xi, \eta), \tag{3.2}$$

where χ_{kl} are either the Proriol or the Appell polynomials discussed in Section 2, and the coefficients $b_{kl}^{(i)}$ are computed by solving the Vandermonde system. As expected, the results are independent of the choice of basis functions. Typical values of the condition number of the Vandermonde matrix,

$$\sigma(\mathbf{V}) = (|\lambda_{\max}|/|\lambda_{\min}|)^{1/2}, \tag{3.3}$$

are shown in Table 1, where $\lambda_{\max}$ and $\lambda_{\min}$ are the eigenvalues of $\mathbf{V}$ with the largest and smallest absolute values, respectively. As expected on account of orthogonality, the condition number for the Appell polynomials is significantly larger than that for the Proriol polynomials. Calculating the Lebesgue constant takes from a few seconds for small values of m, up to several minutes when $m = 9$ on a desktop computer with a 2.4 GHz processor running Linux.

TABLE 1 *Condition number, $\sigma(\mathbf{V})$, for the Vander-monde matrix using the Proriol or Appell polynomials as basis functions*

m	N	Proriol	Appell
2	6	3.57	7.31
3	10	6.62	22.0
4	15	9.52	110
5	21	17.8	664

TABLE 2 *Lebesgue constant, Λ_N, for the Lobatto triangle (LT), the Chen and Babuška points (CB), the Hesthaven points (H) and the Taylor et al. Fekete points*

m	N	LT	CB	H	Fekete
3	10	2.11	2.11	2.11	2.11
6	28	3.87	3.79	4.08	4.17
9	55	7.39	6.80	6.87	6.80

Table 2 shows the Lebesgue constants for the Lobatto triangle grid, the Fekete points tabulated by Taylor *et al.* (2000) together with the Chen & Babuška (1995) and the Hesthaven (1998) distributions. The values quoted by Hesthaven correspond to distributions with the edge nodes located at the zeros of the Lobatto polynomial. When $m = 3$, the Lobatto and Fekete distributions are identical, having one interior node at the centroid of the triangle. The results show that, for $m = 6$, the Lebesgue constant for the Lobatto triangle is in fact lower than that for the Fekete distribution.

As a further test of the interpolation accuracy, we consider the infinity norm

$$L_\infty(f) = \| P_N - f \|_\infty \equiv \max_{\mathbf{x} \in T} |P_N(\mathbf{x}) - f(\mathbf{x})|, \tag{3.4}$$

for a candidate test function $f(\xi, \eta)$, where P_N is the mth-degree interpolating polynomial over the N nodes. The infinity norm was computed by finding the maximum error over the whole of the standard triangle discretized into a large number of mesh points. Table 3 shows the infinity norm for a variety of test functions and various degrees of interpolation, m. Of particular interest is the generalized Runge function, defined as

$$f_R(\hat{\xi}, \hat{\eta}) = \frac{1}{1 + 25(\hat{\xi} - \hat{\xi}_c)^2} \frac{1}{1 + 25(\hat{\eta} - \hat{\eta}_c)^2} \tag{3.5}$$

over the equilateral triangle with sides of unit length, where $(\hat{\xi}_c, \hat{\eta}_c) = (1/2, 1/2\sqrt{3})$ is the centroid of the triangle. The mapping to the standard triangle in $\xi\eta$ space is performed using (2.9). The 1D counterpart of this function allows an exacting test of interpolation performance, where the accuracy of the uniform grid rapidly worsens as the number of nodes is increased (e.g. Pozrikidis, 1998, p. 278; Pozrikidis, 2005). In two dimensions, we find a similar poor performance in approximating (3.5) over the standard triangle using a uniform grid. For the first two functions given in Table 3, the Lobatto triangle interpolation performs as well as, or only slightly worse than, the Fekete interpolation. Interestingly,

TABLE 3 *Infinity norm, $L_\infty(f)$, over the Lobatto triangle for various functions, including the extended Runge function, f_R, defined in the text. The figures shown in parentheses are for the Fekete points*

m	$f = \sin(5\xi)\cos(5\eta)$	$f = e^{2\xi}\cos(10\eta)$	$f = f_R(\xi, \eta)$
1	1.3	9.1	0.93
2	0.87	7.1	0.65
3	0.49 (0.49)	3.6 (3.6)	0.35 (0.35)
4	0.46	3.0	0.37
5	0.092	1.4	0.14
6	0.089 (0.089)	0.56 (0.47)	0.16 (0.13)
7	0.010	0.219	0.087
8	8.78×10^{-3}	0.064	0.040
9	7.3×10^{-4} (6.3×10^{-4})	0.036 (0.024)	0.060 (0.045)

for both $m = 6$ and 9, the Lobatto interpolation performs better than the Fekete interpolation for the more challenging Runge function.

As a final topic, we consider the Lobatto triangle integration quadrature for a non-singular function $f(\xi, \eta)$, expressed by

$$\iint_T f(\xi, \eta)\, d\xi\, d\eta \approx \sum_{i=1}^N f_i w_i, \tag{3.6}$$

where f_i are the function values at the N Lobatto triangle nodes and the integration weights, w_i, are given by

$$w_i = \iint_T \psi_i(\xi, \eta)\, d\xi\, d\eta. \tag{3.7}$$

Considering (3.2) and making use of the zero-mean property

$$\iint_T \chi_{kl}\, d\xi\, d\eta = 0, \tag{3.8}$$

for $k > 0$ and $l > 0$, we derive the simple result

$$w_i = \frac{1}{2} b_{00}^{(i)}, \tag{3.9}$$

independent of the choice of basis functions. As expected, the Lobatto quadrature integrates polynomials of degree m or less, but not higher, exactly. Quadrature weights are listed in Table 4 for several values of m. The displayed node positions, ξ_i and η_i, correspond to points lying within the shaded region of the equilateral triangle shown in Fig. 9. Weights are the same for the points in the same respective positions within the remaining unshaded triangles. The value of ρ_i listed in the table enumerates the total number of points carrying the same weight as node i, including itself.

TABLE 4 *Integration quadrature weights, w_i, based on formula (3.9), for various polynomial degrees m*

|	i	ρ_i	ξ_i	η_i	w_i
$m = 3$	1	3	0.000000	0.000000	0.00833333
	2	6	0.276393	0.000000	0.04166667
	3	1	0.333333	0.333333	0.22500000
$m = 4$	1	3	0.000000	0.000000	−0.00122595
	2	6	0.172673	0.000000	0.02369070
	3	3	0.224224	0.224224	0.10017191
	4	3	0.500000	0.000000	0.02033931
$m = 5$	1	3	0.000000	0.000000	0.00302660
	2	6	0.117472	0.000000	0.00589836
	3	3	0.158286	0.158286	0.06341288
	4	6	0.357384	0.000000	0.01565288
	5	3	0.413304	0.173392	0.05712472
$m = 6$	1	3	0.000000	0.000000	−0.00148086
	2	6	0.084888	0.000000	0.00752218
	3	3	0.116821	0.116821	0.02684295
	4	6	0.265576	0.000000	0.00642726
	5	6	0.315421	0.134734	0.04583453
	6	1	0.333333	0.333333	0.02875392
	7	3	0.500000	0.000000	0.01215198
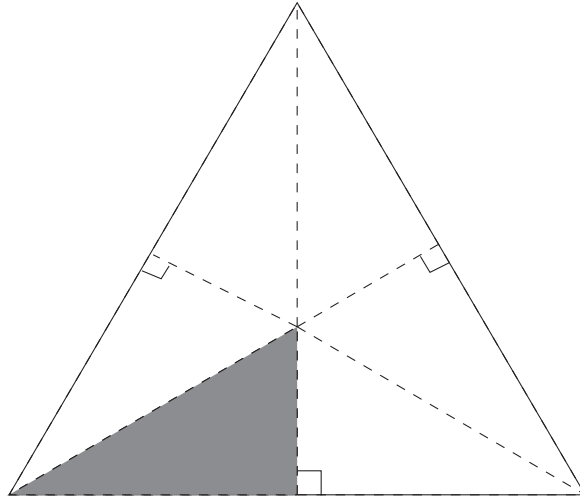
FIG. 9. Quadrature weights are catalogued for nodes lying in the shaded region of the equilateral triangle.

4. Discussion

We have presented a new node distribution for interpolating a function over a triangle. Our primary concern has been to devise a relatively simple node pattern, which is straightforward to generate, but does not over-compromise the interpolation accuracy. Previous high-accuracy schemes demand a fair amount of effort to construct the node positions (e.g. Chen & Babuška, 1995; Hesthaven, 1998; Taylor *et al.*, 2000).

The new node distribution, coined the Lobatto triangle, presents a simple, easy-to-implement interpolation scheme. Edge nodes are positioned at the zeros of the Lobatto polynomials, while the interior nodes are generated by constructing barycentric coordinate lines inside the triangle, and then averaging the coordinates of the vertices of particular internal triangles. Lebesgue constants computed for this new distribution are competitive with those of the more complicated node configurations. Notably, the Lobatto triangle grid outperforms both the Fekete and the Hesthaven distributions for polynomials of degree 6, and is only marginally inferior to the node distribution discussed by Chen and Babuška. The accuracy of the Lobatto triangle distribution was confirmed by computing the infinity norm for a range of sample functions. In particular, the Lobatto triangle scheme performs better when interpolating the generalized Runge function than its counterpart based on the Fekete points.

We noted a connection between interior Fekete points and the zeros of the Lobatto polynomials, and showed that for the case $m = 6$, all nodes can be constructed systematically with the exception of the three near-corner points. These points were accounted for by moving them a small distance to a clearly identifiable location. The result of this small modification is a node distribution which is easy to generate at the expense of only a small increase in the Lebesgue constant.

Finally, we have tabulated the integration weights corresponding to the set of Lobatto triangle base points.

In summary, the Lobatto triangle grid provides us with an accurate and competitive strategy for interpolation over the triangle. Its straightforward implementation makes it an attractive choice for use in spectral element implementations, such as those arising in hydrodynamics.

Acknowledgements

REFERENCES

BOS, L. (1983) Bounding the Lebesgue function for Lagrange interpolation in a simplex. *J. Approx. Theory*, **38**, 43–59.

BOS, L. (1991) On certain configurations of points in $\mathbf{R}^n$ which are unisolvent for polynomial interpolation. *J. Approx. Theory*, **64**, 271–280.

CHEN, Q. & BABUŠKA, I. (1995) Approximate optimal points for polynomial interpolation of real functions in an interval and in a triangle. *Comput. Methods Appl. Mech. Eng.*, **128**, 405–417.

FEJÉR, L. (1932) Lagrangesche interpolation und die zugehorigen konjugierten punkte. *Math. Ann.*, **106**, 1–55.

HESTHAVEN, J. S. (1998) From electrostatics to almost optimal nodal sets for polynomial interpolation in a simplex. *SIAM J. Numer. Anal.*, **35**, 655–676.

KARNIADAKIS, G. E. & SHERWIN, S. J. (2004) *Spectral/hp Element Methods for CFD*, 2nd edn. Oxford: Oxford University Press.

POZRIKIDIS, C. (1998) *Numerical Computation in Science and Engineering.* Oxford University Press.

POZRIKIDIS, C. (2005) *Introduction to Finite and Spectral Element Methods Using Matlab.* Chapman & Hall/CRC.

PRORIOL, J. (1957) Sur une famille de polynomes à deux variables orthogonaux dans un triangle. *C. R. Acad. Sci. Paris*, **245**, 2459–2461.

SUETIN, P. K. (1999) *Orthogonal Polynomials in Two Variables.* Gordon & Breach.

TAYLOR, M. A., WINGATE, B. A. & VINCENT, R. E. (2000) An algorithm for computing Fekete points in the triangle. *SIAM J. Num. Anal.*, **38**, 1707–1720.